Indian Journal of Chemistry
Vol. 57A, July 2018, pp. 887-895

A novel electrochemical biosensor for the detection of ethambutol

Rajasekhar Chokkareddy, Natesh Kumar Bhajanthri & Gan G Redhi*

Department of Chemistry, Durban University of Technology, Durban, South Africa 4000

Email: redhigg@dut.ac.za/ chokkareddys@gmail.com

A glassy carbon electrode (GCE) has been fabricated with zinc oxide nanoparticles (ZnONPs) and reduced graphene oxide (RGO) immobilized with horseradish peroxidase enzyme (HRP) for the voltammetric determination of ethambutol. Electrochemical behaviour of ethambutol has been studied with cyclic voltammetry and differential pulse voltammetry. The HRP-ZnONPs-RGO-GCE exhibits high electrooxidation of ethambutol in phosphate buffer solution at pH 7.0 and the electrochemical signal is significantly enhanced. In addition, the proposed biosensor has been characterized by transmission electron microscopy, Fourier transform infrared spectroscopy and X-ray diffraction. The HRP-ZnONPs-RGO-GCE shows an oxidation peak at –0.2 V with CV. Under the optimized conditions, the DPV technique gave good limit of detection and limit of quantification values of 0.0214 μM and 0.6713 μM respectively. The HRP-ZnONPs-RGO-GCE shows excellent background current stability and gives reliable performance with pharmaceutical samples in the terms of sensitivity, reproducibility and repeatability.

Keywords: Electroanalytical chemistry, Biosensors, Ethambutol, Cyclic voltammetry, Different pulse voltammetry

Tuberculosis (TB) is a major comprehensive health disease, caused by the *Mycobacterium tuberculosis*[1,2]. In recent years, TB affected 9.6 million people and caused 1.5 million deaths, according to the World Health Organization[3]. People with active tuberculosis are required to take several types of medicines like isoniazid, pyrazinamide, rifampicin and ethambutol (ETB) for many months to eradicate the infection and prevent development of antibiotic resistance[4]. Generally, these residual drugs are unaffected by conventional water treatment processes employed by sewage treatment plants (STP) and the presence of unmetabolized drugs in water can contribute in producing drug resistant bacteria[5]. Many methods have been developed for the determination and quantification of ETB in different matrices[6], such as tandem mass spectrometry/ liquid chromatography[7-9], colorimetry[10], chemiluminescence[11,12], high performance liquid chromatography[13], pharmaceutical formulations[14,15], fluorimetry[16] and micellar electrokinetic capillary chromatography (MEKC)[17]. However, these methods need multistep extraction procedures, and selective detectors which not are readily available in third world countries.

Electrochemical method is one of the most promising analytical methods due to its cost-effectiveness, simplicity, rapidity and potential for *in situ* drug monitoring. Nanostructured materials and metal oxides are widely used in electrode modifications due to their wide range of potential applications. Reduced graphene oxide (RGO) is a superior electrode material for biosensors and electrochemical sensors due to its nano-scaled dimensions and unique properties, such as high electrical conductivity (550 S cm^{-1}), good electrochemical stability and high surface-to-volume ratio with the theoretical specific surface area of 2630 m^2 g^{-1}. RGO is highly hydrophilic because of the rich oxygen containing groups (hydroxyl, carboxyl, carbonyl and epoxide groups) on the basal planes and edges of carbon atoms[18,19]. The large surface area and high electrical conductivity of RGO usually causes increase of background currents which become the primary limiting factor for trace analyte detection. RGO and metal oxides nanoparticles show good catalytic properties, which makes them suitable for enhancing the electron transfer between the analyte and electrode surfaces[20]. Horseradish peroxidase (HRP) enzymes are widely used in biosensors and electrochemical biosensors. The HRP exhibits a comparatively less specificity towards electron donor substances and shows good efficiency and rich stability for different biosensors. The electrochemical reaction of ETB potential is separated on the ZnONPs-RGO-GCE, which involves the electrostatic interaction of the electrode surface with the analyte[21]. The HRP-ZnONPs-RGO-GCE contains rich electron groups in its backbone, where the HRP enzyme acts both as electron source and multivalent

nature reaction sites[22]. Moreover, π–π stacking interactions between HRP and conjugated structure of RGO result in an ability to strongly adsorb target species to increase the surface concentration and improve the sensitivity of ETB determination[23, 24]. The (2S)-2-[[(2S)-1-hydroxybutan-2-yl] amino ethyl amino] butan-1-ol is converted to (2S)-2-[[(2S)-1-hydroxybutan-2-yl] amino ethyl amino] butan-1-one. In this context, the main objective of this work was to develop an accurate method as well as precise validation of the new nanocomposite immobilized with HRP, for the determination of ETB in pharmaceutical formulations.

Materials and Methods

Cyclic voltammetry (CV) and differential pulse voltammetry (DPV) were recorded by using a 797 VA Computrace from Metrohm (Herisau, Switzerland) equipped with the Computrace 1.31 software. The electrochemical measurements were obtained by employing a conventional three-electrode system with GCE as working electrode, Ag/AgCl (sat. KCl) as reference electrode, and platinum wire as counter electrode. FT-IR spectra were collected on a Varian 800 FTIR Scimitar series spectrometer in transmission mode. Transmission electron microscopy (TEM) JEM-2100 (model LaB6) was used for morphology studies. Thermogravimetric analysis (TGA) was carried out using a TGA/DSC1SF (model 1346) supplied with a STAR^e software version 9.20 (Mettler toledo). A digital pH ion meter (Crison model 2000) was used to measure the pH of the buffer solutions, used as the supporting electrolyte in electrochemical measurements. All the electrochemical measurements were carried after purging the samples with nitrogen gas, for about 5 min. The stock solution and buffer solutions were kept in the refrigerator at 4 ^oC.

Pure analytical grade ethambutol, horseradish peroxidase enzyme and MWCNTs (O.D.: 6-9 nm; L: 5 μM) were purchased from Sigma Aldrich. Sodium hydroxide, N, N-dimethylformamide (DMF), disodium hydrogen phosphate, sodium dihydrogen *ortho*-phosphate, ethanol, sulphuric acid, ascorbic acid, sucrose, glucose, sodium chloride and $ZnCl_2$ were purchased from Capital Lab suppliers (Durban, South Africa).

Synthesis of ZnONPs

ZnONPs was prepared according to the previous report[25] with a slight modification using 8.17 g of $ZnCl_2$ (0.4 M) dissolved in 150 mL ethanol. This solution was kept under constant stirring using the magnetic stirrer to completely dissolve the zinc chloride for 45 min. In another vessel, 4.48 g (0.8 M) of KOH was dissolved in 100 mL of ethanol to obtain an aqueous ethanol solution of KOH. The $ZnCl_2$ solution was taken in a beaker and the 0.8 M KOH solution was added dropwise under constant magnetic stirring for 2 h. The beaker was sealed and the solutions were allowed to settle overnight. The solution was then separated carefully and centrifuged for 5 min, and thereafter the precipitate was removed. Furthermore, the precipitated ZnO nanoparticles were washed with deionized water several times and dried at 50 °C in an oven. Due to the drying, the $Zn(OH)_2$ was completely converted in to ZnO.

Modification of HRP-ZnONPs-RGO-GCE

The bare GCE was carefully polished to a mirror-like plane with 0.3 μM alumina powder. It was then rinsed with deionized water, followed by successive sonication in 1:1 ethanol and deionized water mixture for 15 min respectively. For the preparation of HRP-ZnONPs-RGO-GCE, 30 mg ZnONPs and 30 mg RGO were dispensed into 15 mL of N, N-dimethyl formamide (DMF) followed by ultrasonication for about 90 min, to obtain a homogeneous suspension of ZnONPs-RGO of the desired concentration (0.40%, *w/v*). Then, 5.0 μL of ZnONPs-RGO suspension (8.00%, *w/v*) was coated onto the surface of GCE and dried in the oven at 50 ^oC for 10 min. Thereafter, ZnONPs-RGO-GCE was dipped into HRP solution for 1 h and kept undisturbed at 4 °C for about 30 min for complete enzyme immobilization and then allowed to dry at ambient temperature for 10 min. The obtained electrode was designated as HRP-ZnONPs-RGO-GCE. For comparison, a similar procedure was used to prepare the ZnONPs-RGO-GCE and RGO-GCE. Finally, HRP-ZnONPs-RGO-GCE was used for the electrochemical measurements.

Results and Discussion

Morphological and structural characterization of HRP-ZnONPs-RGO-GCE

TEM images were studied to find the exact particle size of ZnONPs. Figure 1(a) shows the TEM image of ZnONPs, which are nearly spherical and monodispersed, with the particle diameter approximately 35 nm and matches with XRD data[26, 27]. The TEM image of RGO shows the sheets consist of a few layers, each fixed with wrinkled structure due to the sheet folding (Fig. 1(b))[28-31]. The TEM image of the ZnONPs-RGO

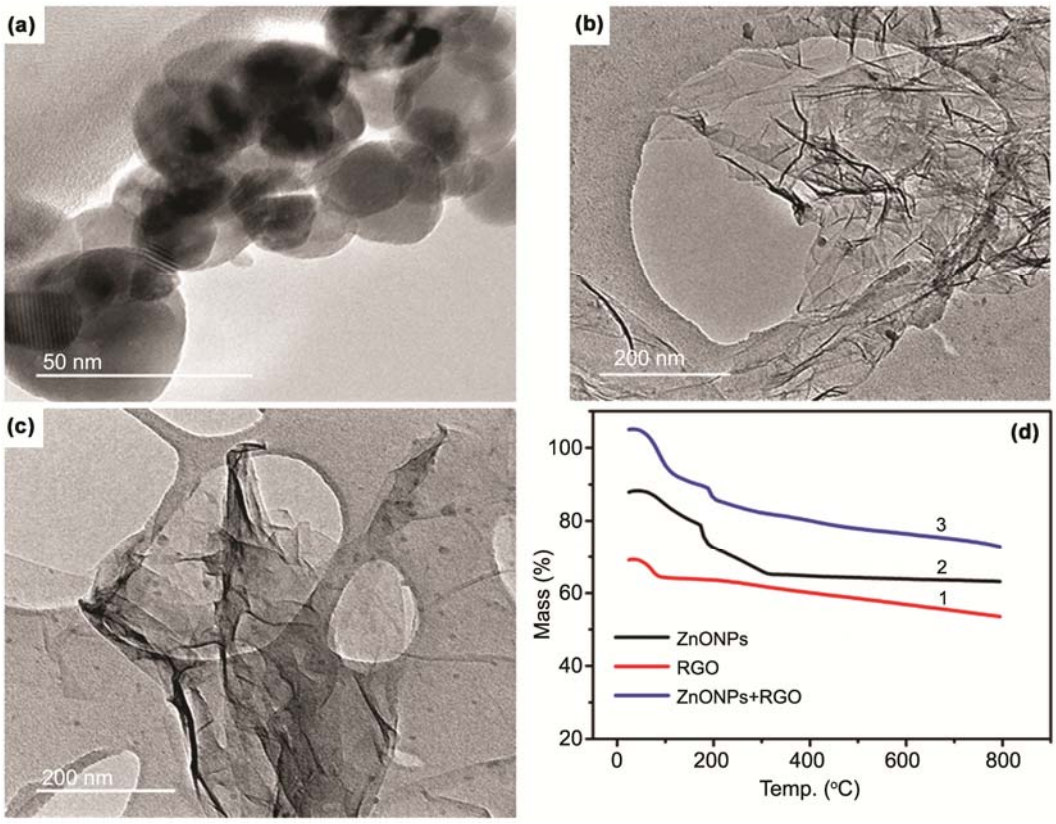

Fig. 1 — TEM images of (a) ZnONPs, (b) RGO, and (c) ZnONPs-RGO, and, (d) TGA curves for (1) RGO, (2) ZnONPs, and (3) ZnONPs-RGO.

clearly shows that the ZnO nanoparticles are agglomerated and distributed homogeneously on the RGO sheet (Fig. 1(c)). Our study revealed that such a complex lends itself as a potential precursor for ZnONPs synthesis through thermal decomposition. TGA analyses of the ZnONPs, RGO and ZnONPs-RGO were conducted from room temperature to 800 °C. Figure 1(d) shows the TGA curves for a typical precursor; at 200 °C the ZnONPs shows high weight loss due to the evaporation of water absorbed on the surface[30]. The maximum loss occurs at 375 °C, which also indicates a high rate of degradation of ethyl alcohol into volatile combustible products[31]. RGO exhibits one clear step of weight loss below 150 °C, which relates to the loss of water molecules[32]. Furthermore, the ZnONPs-RGO shows a minor weight loss below 100 °C due to the release of moisture. The loss of weight at 200 °C may be attributed to desorption of moisture and solvents[33].

FT-IR studies were carried out in order to determine the purity and nature of the metal oxide nanoparticles. The metal oxide nanoparticles generally give adsorption bands in fingerprint region

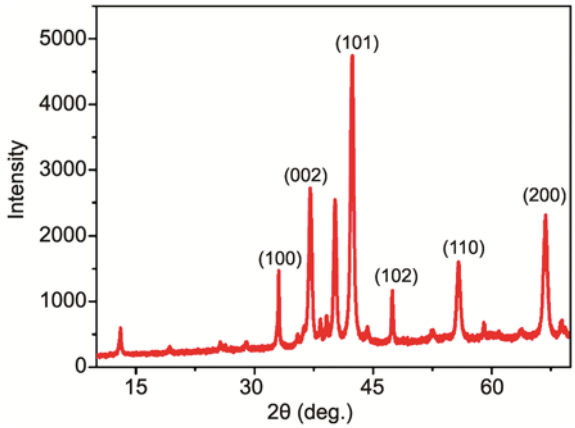

Fig. 2 — XRD pattern of ZnONPs.

below 1000 cm^{-1} arising from inter-atomic vibrations. ZnONPs shows adsorption bands at 440–500 cm^{-1}, indicating the Zn-O stretching[34]. The peaks at 2350 and 3450 cm^{-1} specify the presence of C=O and –OH residues, which may be due to the atmospheric moisture and CO_2 respectively[31,35]. The peaks located at 2937 and 2885 cm^{-1} are due to the symmetric and asymmetric C-H bonds respectively[36]. The XRD pattern of the synthesized ZnONPs is shown in Fig. 2.

The diffraction peaks are located at 32.85° (100), 38.23° (002), 42.36° (101), 47.62° (102), 56.35° (110), and 64.38° (200) respectively. Furthermore, the peak intensity is narrow and sharp, and confirms the excellent crystallinity of ZnONPs. The diffraction peaks of the ZnONPs correspond to the specific hexagonal wurtzite structure[31,37]. The crystallites undergo a reorientation with the (002) orientation being favoured, while the (100) peak intensity decreases. The nanoparticle size calculated by using the Debye-Scherer formula was found to be approximately 35 nm.

Electrochemical characterization and effect of deposition time

The electrochemical behaviour of ETB on the bare GCE, RGO-GCE, ZnONPs-RGO-GCE and HRP-ZnONPs-RGO-GCE is shown in Fig. 3(a). The CV performance of 0.1 mM ETB in 0.1 M PBS (pH 7.0) in the positive scan direction showed a quasi-reversible pair corresponding to redox reactions. The bare GCE showed an oxidation peak at –0.12 V and a reduction peak at –0.22 V with a peak current of 14 µA, which may be attributed to the poor electrochemical activity on the bare GCE (curve 1). RGO-GCE and ZnONPs-RGO-GCE also showed anodic and cathodic peaks at –0.12 V and –0.22 V with 25 µA and 85 µA peak currents respectively (Supplementary Data, Fig S1). On the other hand, the HRP-ZnONPs-RGO-GCE showed sharp anodic and cathodic peaks with a peak current of 130 µA. There was also a discrete increase in the peak current for each step of electrode modification, which can be justified via Randles-Sevick equation[38],

$$i_{pa} = 2.69\,x10^5 AC_0 n^{3/2} {D_R}^{1/2} v^{1/2} \quad \ldots(1)$$

where i_{pa} is the anodic peak current, A is the surface area of the electrode, C_0 is the concentration of ethambutol, n is the number of electrons transferred, D_R is the diffusion coefficient and v is the scan rate. By using the anodic peak current from Fig. 3(a) for the bare GCE (curve 1), D_R may be calculated and then along with the anodic peak current for the modified GCE, the surface area of the HRP-ZnONPs-RGO-GCE may be calculated. The surface area of HRP-ZnONPs-RGO-GCE was found to be 13.12 mm^2 in comparison to bare GCE of 3.14 mm^2. Hence, the fabricated electrode provides an extremely large enhancement of the anodic and cathodic currents as observed. There was significant enhancement in current response as shown

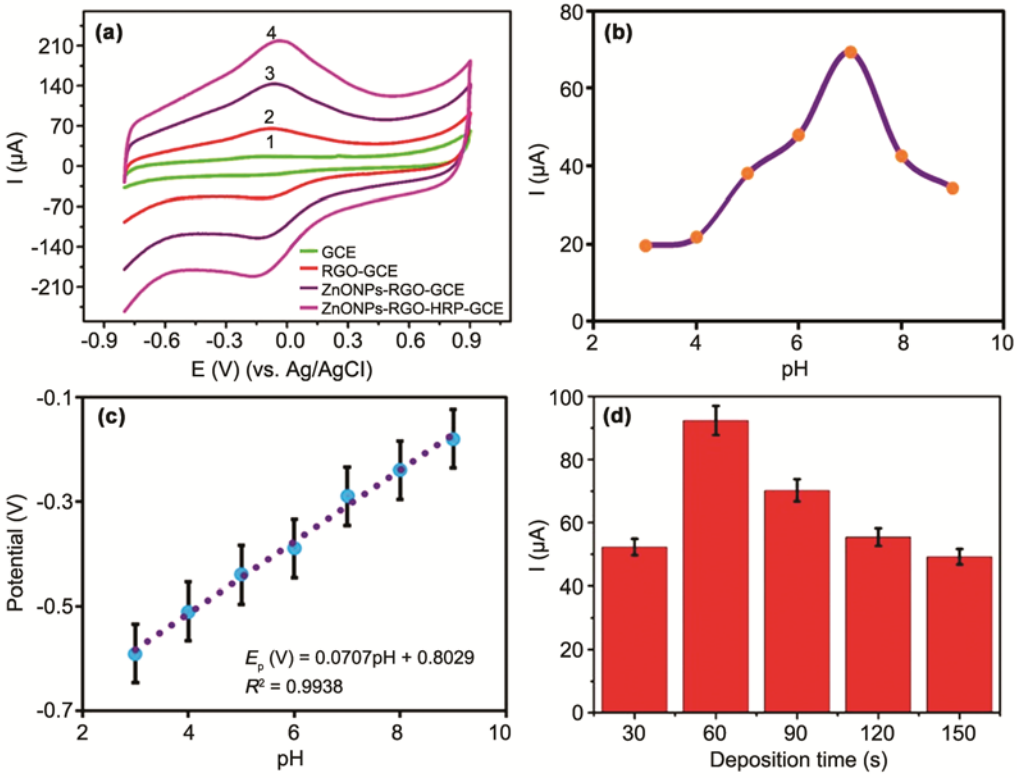

Fig. 3 — (a) Cyclic voltammograms of 0.1 mM ETB at bare GCE (1), RGO-GCE (2), ZnONPs-RGO-GCE (3), and, HRP-ZnONPs-RGO-GCE (4). (b) Peak potential and current response with respect to change in pH (3–9) with 0.1 mM ETB. (c) Plot of peak potential (E_p) of anodic wave versus pH (pH 3–9). (d) Effect of varying deposition times (30, 60, 90, 120, and 150 s) on peak current.

in Fig. 3(a). The effect of deposition time from 30–150 s is shown in Fig. 3(d). In addition, the sensitivity was improved to provide a longer deposition time. Also, an increase in the upper detection limits, due to the electrode surface saturation in the high concentration region was observed. When the deposition time became longer than 60 s, the peak currents decreased gradually which may be due to the working electrode surface saturation. Due to the increased sensitivity, an optimized deposition time of 60 s was used throughout the experiment.

Effect of pH on the electrochemical behaviour of ETB at HRP-ZnONPs-RGO-GCE

The electrochemical redox reaction was influenced by protons in the electrode reaction process of ETB, and hence, the effect of the solution pH was investigated. The effect of pH on the current responses of HRP-ZnONPs-RGO-GCE towards 0.1 mM of ETB was investigated within the pH range of 3.0–9.0. Figure 3(b) shows that the oxidation peak currents gradually increased with the increase in pH from 3.0 to 7.0. This phenomenon may be attributed to the high concentration of protons in the solution. The anodic peak current of ETB reaches a maximum at pH 7.0. The peak potential E_{pc} shifted to higher negative potentials when the pH was increased, with correlation coefficient R^2 = 0.993 (Fig. 3(c)). The HRP-ZnONPs-RGO-GCE showed electron transfer accompanied by an equal number of protons in the electrode reaction. Therefore, pH 7.0 was selected as the optimum solution pH for the entire study.

Effect of enzyme incubation time

The enzyme incubation time of the HRP-ZnONPs-RGO-GCE is an important parameter for the determination of ETB. The enzyme incubation time was investigated in the range of 5–25 min at room temperature, and then the corresponding current responses were measured by DPV (Supplementary Data, Fig. S2). The current response increased gradually with prolonged incubation time and attained maximum at 15 min. Above 15 min, the peak current response gradually decreased with increase in incubation time. This suggests that the fabricated electrode reaches saturation point at 15 min. Hence, 15 min was selected as the optimum incubation time for the determination of ethambutol.

Effect of scan rates on the electrochemical behaviour of ETB at HRP-ZnONPs-RGO-GCE

Figure 4(a) shows the effect of scan rate on the peak current and peak potential of ETB at HRP-ZnONPs-RGO-GCE. For this investigation, the electrochemical reaction of ETB at the HRP-ZnONPs-RGO-GCE were studied using cyclic voltammetry at a relatively low scan rate from 0.01–0.1 mV s^{-1}, in the presence of 0.1 mM PBS (pH 7.0). As shown in Fig. 4(b), when the

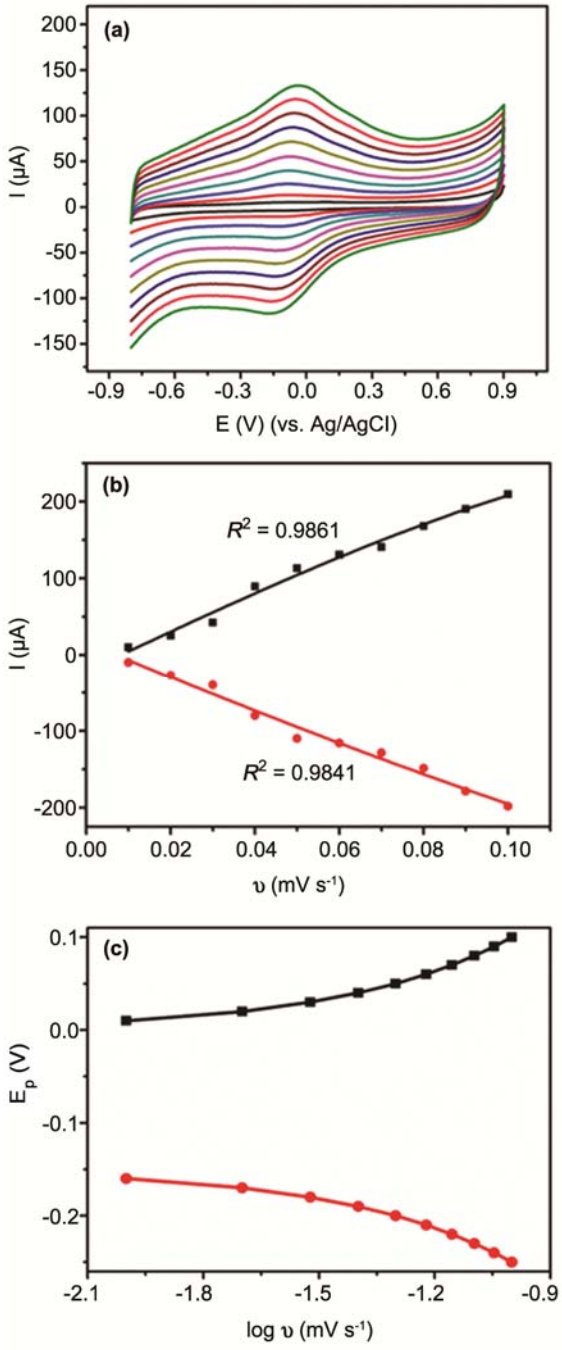

Fig. 4 — (a) Cyclic voltammograms of 0.1 mM ETB on the surface of HRP-ZnONPs-RGO-GCE at varying scan rates in PBS buffer of pH 7.0. [(1) 0.01; (2) 0.02; (3) 0.03; (4) 0.04; (5) 0.05; (6) 0.06; (7) 0.07; (8) 0.08; (9) 0.09; (10) 0.1 mV s^{-1}]. (b) Dependence of anodic and cathodic peak current on scan rate. (c) Variation of peak potential versus log scan rate from 0.01 to 0.1 mV s^{-1}.

scan rate was varied from 0.01–0.1 mV s^{-1} in 0.1 mM of ETB, a linear dependence of the redox response upon the scan rate (ν) was observed, demonstrating an adsorption controlled process[39]. The results show that the anodic and cathodic peak current increased with an increase in the scan rate, indicating the electrochemical oxidation and reduction process of ETB at the HRP-ZnONPs-RGO-GCE. Based on the above results, it can be reasonably assumed that ETB was firstly absorbed on the surface of the electrode and then the electrode reaction occurs. Further, based on the Laviron model[40], the electron transfer coefficient α, and the apparent heterogeneous charge transfer rate constant k_s, can be estimated from cyclic voltammetry using the deviation of the anodic and cathodic peak potentials as a function of the logarithm of scan rates. At high scan rates this theory calculated a linear dependence of E_{pvs} and log v, which can be used for the determination of kinetic parameters like α and k_s from the slope and intercept plots shown in Fig. 4(b). The plot of E_P against log v from CV of ETB at HRP-ZnONPs-RGO-GCE in PBS (pH 7.0) is shown in Fig. 4(c). From the slope of the linear plots of $E_P = f(\log v)$, the cathodic peak is found to be $-2.3RT/\alpha nF$ and anodic peak $2.3RT/(1-\alpha)nF$. On substituting the two peak values in Eq. (2), the charge transfer coefficient α was found to be 0.63 and the electron transfer constant was estimated to be $k_s = 2.93\ s^{-1}$.

$$\log k_s = \alpha\log(1-\alpha) + (1-\alpha) - \log(RT/nFv) - \alpha(1-\alpha)(nF\Delta E_P/2.3RT) \quad \ldots (2)$$

where ΔE_P is $(E_{Pa}-E_{Pc})$, α is the transfer coefficient, ν is the potential scan rate (mV s^{-1}), k_s is the heterogeneous electron transfer rate constant (s^{-1}) and R and T have their usual meanings.

Stability studies

The electrochemical oxidation and reduction reactions of ETB at the HRP-ZnONPs-RGO-GCE were studied using the CV and DPV techniques to evaluate the repeatability and reproducibility as these are critical parameters for a biosensor's performance. The electrode-to-electrode reproducibility gave a satisfactory RSD value of 2.83% for the detection of 0.1 mM ETB at three independently fabricated electrodes. The repeatability of the biosensor was also examined by monitoring the current response to 0.1 mM ETB five times. The RSD was 1.93%, indicating a remarkable reproducibility of the fabricated electrode. The long term storage stability of the HRP-ZnONPs-RGO-GCE was determined by measuring the current response of 0.1 mM ETB over a period of 20 days. The fabricated electrode was stored in 0.1 M PBS (pH 7.0) at 4 °C when not in use. The stability response of the HRP-ZnONPs-RGO-GCE was observed as a plot of $(i\text{-}i_0)/i_0$ (where i_0 is the current response of modified HRP-ZnONPs-RGO-GCE, i is the current response at any storage time, $(i\text{-}i_0)$ is the change in the response current at any storage time) versus the time (in days) (Supplementary Data, Fig. S3). The HRP-ZnONPs-RGO-GCE showed good stability up to five days, with the current response of 84%. After 15 days, the activity was 72%, i.e., a decrease of only 12% in current response after 15 days. Based on these results, it is proposed that the biosensor showed good long-term stability.

Calibration plots and detection limit

The analytical curve for the HRP-ZnONPs-RGO-GCE, and quantitative analysis of 0.1 M ETB were obtained by DPV under the optimized experimental conditions. With successive additions of ETB, the peak currents increased linearly with increasing concentration of ETB; the corresponding calibration curve is presented as an inset in Fig. 5. The calibration curves are linear over concentration range of 2–32 μM for DPV. Using HRP-ZnONPs-RGO-GCE, the detection of ETB was in the potential

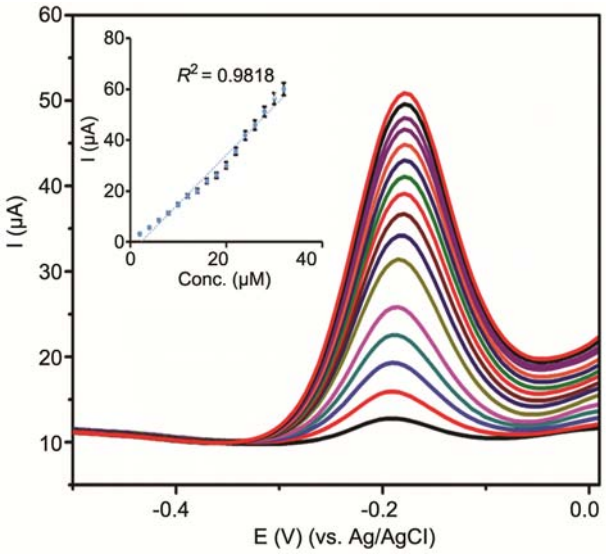

Fig. 5 — DPVs of HRP-ZnONPs-RGO-GCE obtained in a linear range of 2–32 μM of ETB in PBS (pH 7.0) at scan rate of 0.015 mV s^{-1}. {Inset: plot shows the linear dependence of I_{pc} versus [ETB]}.

Table 1 — Comparison of present electrochemical biosensor with other described methods for the detection of ETB in pharmaceutical samples

Electrode	Technique	Detection limit (μM)	Buffer (pH)	Ref.
Carbon electrode	FIA	100	NaOH (12.0)	42
Platinum electrode	CE	24.2	Sodium tetraborate (8.03)	14
Au-PVP-Ag-PANSA-CYP2E1	CV & DPV	0.7	PBS (7.0)	43
Tyr-GCE	CV & DPV	9.61	PBS (7.0)	44
Gold microelectrode	CV & SWV	4.73	ACS (4.5)	45
Nafion-MWCNT-SPCE	CV & SWV	8.4	PBS (7.4)	46
HRP-ZnONPs-RGO-GCE	CV & DPV	0.0214	PBS (7.0)	This work

FIA: Flow injection analysis; CE: Capillary electrophoresis; Au/PVP-Ag-PANSA/CYP2E1: Silver nanoparticle/poly(8-anilino-1-naphthalene sulphonic acid); CV: Cyclic voltammetry; DPV: Differential pulse voltammetry; ACS: Acetate buffer solution; Tyr-GCE: Tyrosine modified on glassy carbon electrode; SWV: Square wave voltammetry; Nafion-MWCNT-SPCE: Nafion-multiwalled carbon nanotubes modified screen printed carbon electrode; HRP-ZnONPs-RGO-GCE: Horse radish peroxidase-zinc oxide-reduced graphene oxide modified glassy carbon electrode.

range of –0.5 to 0.0 V under the optimal parameters of pulse amplitude = 0.052 V, pulse time = 0.041 s, scan rate = 0.015 mV s^{-1} and deposition time = 60 s. A well-defined peak was obtained at –0.2 V (vs. Ag/AgCl) with a good linearity (R^2 = 0.9818). The limit of detection (LOD) and limit of quantization (LOQ) were calculated by the signal-to-noise method to be 0.0214 μM and 0.6713 μM respectively. HRP-ZnONPs-RGO-GCE was compared with some other electrodes reported for ETB determination (Table 1). The HRP-ZnONPs-RGO-GCE showed better LOD and LOQ values for ETB than the previously reported sensors.

Interference studies

The interference from the various interfering reductive species was investigated by DPV using 0.1 mM ETB. The interfering species were added in concentrations higher than that normally present in the real samples. The tolerable interference concentration was taken as the measured signal variation which was approximately ±3. Some of the organic compounds such as ascorbic acid, sucrose, glucose and common ions such as Ca^{2+}, K^+, Cl^-, Ag^+, Br^-, Na^+ and SO_3^{2-} had no influence on the determination of ETB (Table 2). According to these results, HRP-ZnONPs-RGO-GCE exhibits negligible interference effect for the determination of ETB.

Determination of ETB in pharmaceutical formulation

Commercially available tablets (fifteen), each containing 300 mg and 500 mg of ETB, were finely powdered with a mortar and pestle. The average weight of five tablets was determined and then transferred into a 25 mL standardized volumetric flask, to which 25 mL of deionized water was added and then ultrasonicated for 60 min. The resulting mixture was successively filtered with Whatman (No. 1) filter paper and the concentration of the samples was diluted and made equal to the working concentration range. The concentration of ETB in the pharmaceutical formulations were determined with DPV, using the calibration curve plot. The results are summarized in Table 3. The recovery percentages varied in the range of 98.5–99.6%, which can be considered to be substantial and very close to the WHO monograph on ETB[41] (not less than 98% and not more than 105% of ETB are contained in labeled samples).

Table 2 — The influence of anions, cations and important biological substances on the peak current of 0.1 mM ETB at HRP-ZnONPs-RGO-GCE

Interferents	Conc. (μM)	Change in current responses (%)
Ascorbic acid	50	–2.06
	100	–3.96
Sucrose	50	–1.32
	100	–2.03
Glucose	50	–1.28
	100	–2.62
Ca^{2+}	50	–0.36
	100	–0.65
K^+	50	–0.64
	100	–1.02
Cl^-	50	–1.20
	100	–2.01
Ag^+	50	–0.86
	100	–1.54
Br^-	50	–0.56
	100	–1.26
Na^+	50	–0.21
	100	–0.50
SO_3^{2-}	50	–0.76
	100	–1.36

Precision and accuracy

The repeatability of the proposed electrochemical biosensor (intra-day precision) was estimated by associating the standard deviations found from the peak

Table 3 — Determination of ETB in various pharmaceutical samples using HRP-ZnONPs-RGO-GCE (n = 5)

ETB (mg)		Recovery (%)	RSD (%)	ETB (mg)		Recovery (%)	RSD (%)
Cert. amt	Found			Added	Found		
Sample 1 (300 mg)	298.7	99.5	1.79	50	49.3	98.6	0.42
Sample 2 (500 mg)	498.2	99.6	1.98	100	98.5	98.5	0.89

area measurements. The standard deviation values varied from 0.58–0.98 for intra-day precision. Inter-day precision analysis was performed on five consecutive days and the obtained standard deviations ranged from 1.12–1.16, which shows good precision of the proposed method. The standard deviation values obtained in this analytical technique compared very favourably with that obtained in the reference material[40]. Accuracy was estimated as a percentage of relative error between the calculated mean concentration and added (spiked) concentration for ETB (Bias %). The values were found to be in the range of 0.58 to 0.98% for inter-day and 0–0.40 for intra-day analysis (Supplementary Data, Table S1).

Conclusions

The ZnONPs-RGO nanocomposite provides an appropriate environment for HRP enzyme attachment and rapid catalytic action. It is facilitated by the electron transfer between the active sites of enzyme and electrode surface. The performance of HRP-ZnONPs-RGO-GCE was significantly improved by the electrochemical oxidation and reduction of ETB as compared with ZnONPs-RGO nanocomposite, GCE and RGO. The proposed biosensor shows a low limit of detection (0.0214 μM) and limit of quantification (0.6713 μM). Based on the detection limit, sensitivity, and stability, the proposed HRP-ZnONPs-RGO-GCE can be used as a reliable routine laboratory technique for monitoring ETB in biological and pharmaceutical samples.

Supplementary Data

Supplementary data associated with this article are available in the electronic form at http://www.niscair.res.in/jinfo/ijca/IJCA_57A(07)887-895_SupplData.pdf.

Acknowledgement

The authors gratefully acknowledge financial support for this work from the Durban University of Technology, Durban, South Africa.

References

1 Rastogi P K, Ganesan V & Azad U P, *Electrochim Acta,* 188 (2016) 818.
2 Chokkareddy R, Bhajanthri N K & Redhi G G, *Int J Electrochem Sci,* 12 (2017) 9190.
3 Cheemalapati S, Chen S M, Ali M A & Al-Hemaid F M, *Colloids Surf B*, 121 (2014) 444.
4 Ghoneim M M, El-Baradie K Y & Tawfik A, *J Pharm Biomed Anal*, 33 (2003) 673.
5 Cheemalapati S, Devadas B & Chen S M, *J Colloid Interface Sci*, 418 (2014) 132.
6 Abolhasani J & Hassanzadeh J, *Luminescence*, 29 (2014) 1053.
7 Hee K H, Seo J J & Lee L S, *J Pharm Biomed Anal*, 102 (2015) 253.
8 Zhou Z, Wu X, Wei Q, Liu Y, Liu P, Ma A & Zou F, *Anal Biochem*, 405 (2013) 6323.
9 Song S H, Jun S H, Park K U, Yoon Y, Lee J H, Kim J Q & Song J, *Rapid Commun Mass Spectrom*, 21 (2007) 1331.
10 Muttil P, Kaur J, Kumar K, Yadav A B, Sharma R & Misra A, *Eur J Pharm Sci*, 32 (2007) 140.
11 Liu Y, Fu Z & Wang L, *Luminescence*, 26 (2011) 397.
12 Xi J, Shi B A, Ai X & He Z, *J Pharm Biomed Anal*, 36 (2004) 237.
13 Gennaro M C, Calvino R & Abrigo C, *J Chromatogr: B*, 754 (2001) 477.
14 Ngece R F, West N, Ndangili P M, Olowu R A, Williams A, Hendricks N, Mailu S, Baker P & Iwuoha E, *Int J Electrochem Sci,* 6 (2011) 1820.
15 Cheemalapati S, Devadas B, Chen S M, Ali M A & Al-Hemaid F M A, *Anal Methods*, 6 (2014) 6774.
16 Wu W Y, Yang J Y, Du L M, Wu H & Li C F, *Spectrochimica Acta Part A: Mol Biomol Spectr*, 79 (2011) 418.
17 Espinosa-Mansilla A, Acedo Valenzuela M I, Muñoz de la Peña A, Salinas F & Cañada F C, *Anal Chim Acta*, 427 (2001) 129.
18 Benvidi A, Nikmanesh M, Dehghan Tezerjani M, Jahanbani S, Abdollahi M, Akbari A & Rezaeipoor-Anari A, *J Electroanal Chem,* 787 (2017) 145.
19 Liu L, Li Y, Tian L, Guo T, Cao W & Wei Q, *Sensors Actuators B,* 211 (2015) 170.
20 Khalil I, Julkapli N, Yehye W, Basirun W & Bhargava S, *Materials*, 9 (2016) 4061.
21 Li G & Miao P, *Springer*, (2013) 5.
22 Ahirwal G K & Mitra C K, *Sensors,* 9 (2009) 881.
23 Alonso Lomillo M A, Kauffmann J M & Arcos Martinez M J, *Biosens Bioelectron*, 18 (2003) 1165.
24 Sun H, Liu Z, Wu C, Xu P & Wang X, *Sci Rep*, 6 (2016) 30905.
25 Srinivasa Rao N & Basaveswara Rao M V, *Am J Mater Sci,* 5 (2015) 66.
26 AbdElhady M M, *Int J Carbohydr Chem,* 2012 (2012) 1.

27 Taunk P B, Das R, Bisen D P & Tamrakar R K, *J Rad Res Appl Sci*, 8 (2015) 433.

28 Ortolani L, Cadelano E, Veronese G P, Degli Esposti Boschi C, Snoeck E, Colombo L & Morandi V, *Nano Lett*, 12 (2012) 5207.

29 Zhang H & Feng P X, *Carbon*, 48 (2010) 359.

30 Moharram A H, Mansour S A, Hussein M A & Rashad M, *J Nanomat,* 2014 (2014) 1.

31 Khalil M I, Al-Qunaibit M M, Al-zahem A M & Labis J P, *Arab J Chem,* 7 (2014) 1178.

32 Loryuenyong V, Totepvimarn K, Eimburanapravat P, Boonchompoo W & Buasri A, *Adv Mater Sci Eng,* 2013 (2013) 1.

33 Becheri A, Dürr M, Lo Nostro P & Baglioni P, *J Nanoparticle Res,* 10 (2008) 679.

34 Kumar H & Rani R, *Phys Astron,* 14 (2013) 26.

35 Zak A K, Majid W H A, Darroudi M & Yousefi R, *Mater Lett,* 65 (2011) 70.

36 Vafaee M & Ghamsari M S, *Mater Lett,* 61 (2007) 3265.

37 Talam S, Karumuri S R & Gunnam N, *ISRN Nanotechnology*, 2012 (2012) 1.

38 Chokkareddy R, Bhajanthri N K & Redhi G G, *Biosensors*, 7 (2017) 1.

39 Mohammadi N, Najafi M & Adeh N B, *Sensors Actuators B*, 243 (2017) 838.

40 Gowda J I & Nandibewoor S T, *Asian J Pharmaceut Sci,* 9 (2014) 42.

41 *Ethambutol, Rifampicin, Isoniazid and Pyrazinamide Dispersible Tablets,* (World Health Organization); http://www.who.int/medicines/publications/pharmacopoeia/QAS07/222rev1/Rif-Iso-Pyraz-dispers. (October 2007).

42 Perantoni C B, Lowinsohn D, Carbogim L G S, Semaan F S & Matos R C, *Electroanalysis,* 23 (2011) 2582.

43 DaSilva J A F, de Castro N V, de Jesus D P, Faria A F, De Souza M V N & de Oliveira M A L, *Electrophoresis*, 31 (2010) 570.

44 Cheemalapati S, Devadas B, Chen S M, Ali M A & Al-Hemaid F M A, *Anal Methods*, 6 (2014) 6774.

45 Lima A E B, Luz Jr G E, Batista N C, Longo E, Cavalcante L S & Santos R S, *Electroanalysis*, 27 (2015) 1.

46 Couto R A & Quinaz M B, *Sensors (Basel)*, 16 (2016) 1.